Supporting Information

Molecular-Level Understanding of Excited States of N-Annulated Rylene Dye for Dye-Sensitized Solar Cells

Changwon Kim,[ab] Tae Wu Kim,[b#] Siin Kim,[ab] Inhwan Oh,[ab] Henrike Wonneberger,[c] Kihwan Yoon,[d] Minseok Kwak,[e] Joonghan Kim,[d] Jeongho Kim,[f] Chen Li,[g] Klaus Müllen,[h] and Hyotcherl Ihee[*ab]

[a]*Department of Chemistry and KI for the BioCentury, Korea Advanced Institute of Science and Technology (KAIST), Daejeon 34141, Republic of Korea*

[b]*Center for Nanomaterials and Chemical Reactions, Institute for Basic Science (IBS), Daejeon 34141, Republic of Korea*

[c]*BASF SE, Carl-Bosch-Strasse 38, Ludwigshafen 67056, Germany*

[d]*Department of Chemistry, The Catholic University of Korea, Bucheon 14662, Republic of Korea*

[e]*Department of Chemistry, Pukyong National University, Busan 48513, Republic of Korea*

[f]*Department of Chemistry, Inha University, Incheon 22212, Republic of Korea*

[g]*School of Environment and Civil Engineering, Dongguan University of Technology, Dongguan, Guangdong Province, P. R. China*

[h]*Max Planck Institute for Polymer Research, Ackermannweg 10, 55128 Mainz, Germany*

[#]*Present address: Chemical Sciences and Engineering Division, Argonne National Laboratory, Lemont, Illinois 60439, United States*

Supporting Information (SI) Figures and Tables

Table of Contents

Supplementary Note 1. Synthesis and characterization of DND

N-Cyclohexyl-4-(4-chloro-2-nitro-phenyl)-1,8-naphthalene dicarboximide

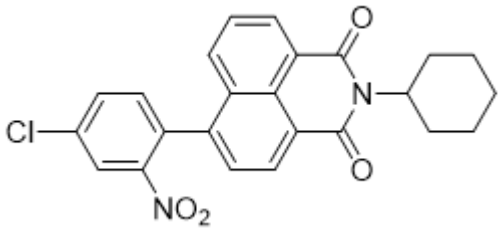

2 g of N-cyclohexyl-4-(4,4,5,5-tetramethyl-1,3,2-dioxaborolane-2-yl)-naphthalene-1,8-dicarboximide (4.93 mmol) and 1.75 g of 1-bromo-4-chloro-2-nitrobenzene (7.40 mmol) were dissolved in 80 mL of toluene. 1.6 g of potassium carbonate (11.6 mmol) dissolved in 8 mL of water, and 0.8 mL of ethanol were added. The solution was purged with argon for 30 minutes. After addition of 800 mg tetrakis(triphenylphosphine)palladium(0) (0.717 mmol), the solution was again purged for 30 minutes with argon. The solution was stirred at 80 °C for 60 h. The reaction mixture was cooled down, washed with water, and extracted with dichloromethane. The reaction mixture was purified via column chromatography on silica gel with dichloromethane:petrol ether (1:1). **Yield**: 700 mg light-yellow solid (32%)

^{1}H-NMR (700 MHz, CD_2Cl_2, 298 K): δ [ppm]: 8.60 - 8.55 (m, 2H), 8.23 (d, J = 2.1, 1H), 7.79 (dd, J = 2.1, 8.2, 1H), 7.74(dd, J = 0.9, 8.4, 1H), 7.70 - 7.66 (m, 1H), 7.59 (d, J = 7.4, 1H), 7.46 (d, J = 8.2, 1H), 5.05 - 4.97 (m, 1H), 2.54 (qd, J = 3.5, 12.5, 2H), 1.90 (d, J = 13.2, 2H), 1.78 - 1.69 (m, 3H), 1.51 - 1.41 (m, 2H), 1.38 - 1.28 (m, 1H).

^{13}C-NMR (176 MHz, CD_2Cl_2, 298 K): δ[ppm]: 164.8, 164.6, 149.8, 141.4, 136.2, 134.4, 134.1, 132.7, 131.5, 130.9, 130.7, 130.4, 128.8, 128.1, 127.5, 125.6, 124.5, 124.3, 29.7, 27.2, 26.1. **IR spectrum (ATR)**: ν_{max} [cm^{-1}] = 3098, 2928, 2848, 1701, 1658, 1594, 1525, 1389, 1346, 1231, 1107, 786. **UV-Vis spectrum (CH_2Cl_2)**: λ_{max} [nm] (ε [$M^{-1}cm^{-1}$])= 340 (16,888). **High Resolution Mass (ESI)**: $[M+H]^+$: calculated: 435.1112, found: 435.1111, discrepancy: -0.1 ppm.

N-Cyclohexyl-4-(4-bis(p-2,4,4-trimethylpentane-2-yl-phenyl)amino-2-nitro-phenyl)-1,8-naphthalene dicarboximide

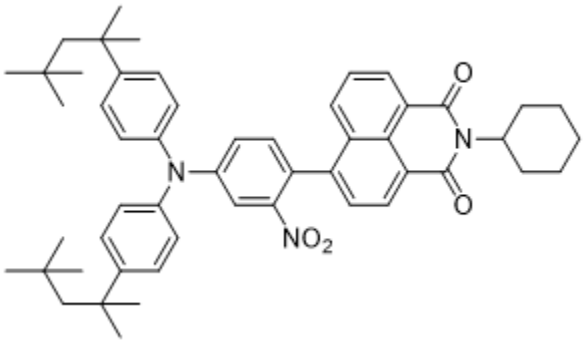

600 mg of N-cyclohexyl-4-(4-chloro-2-nitro-phenyl)-naphthalene-1,8-dicarboximide (1.38 mmol), 815 mg of bis(p-2,4,4-trimethylpentane-2-yl-phenyl)amine (2.07 mmol), 900 mg of caesium carbonate (2.76 mmol), 125 mg of tris(dibenzylideneacetone) dipalladium(0) (0.136 mmol), and 170 mg of 2,2'-bis(diphenylphosphino)-1,1'-binaphthyl (0.273 mmol) were dissolved in 30 mL of anhydrous toluene in a Schlenk tube and stirred under argon at 100 °C for 16 h. The reaction mixture was purified via column chromatography with dichloromethane:petrol ether (1:1). **Yield**: 640 mg yellow solid (64%)

^{1}H-NMR (700 MHz, CD_2Cl_2, 298 K): δ [ppm]: 8.55 (d, J = 7.5, 2H), 7.93 (d, J = 8.4, 1H), 7.71 - 7.66 (m, 1H), 7.62 - 7.58 (m, 2H), 7.41 (d, J = 8.7, 4H), 7.27 (dd, J = 2.5, 8.5, 1H), 7.21 (d, J = 8.5, 1H), 7.17 (d, J = 8.6, 4H), 5.07 - 4.95 (m, 1H), 2.60 - 2.48 (m, 2H), 1.89 (d, J = 13.2, 2H), 1.80 - 1.68 (m, 7H), 1.51 - 1.23 (m, 15H), 0.76 (s, 18H). **^{13}C-NMR (176 MHz, CD_2Cl_2, 298 K)**: δ [ppm]: 165.0, 164.8, 150.3, 147.9, 143.7, 143.3, 133.4, 131.5, 131.3, 130.9, 128.8,128.4, 127.7, 125.8, 124.4, 124.2, 123.6, 123.5, 115.1, 57.6, 38.9, 32.9, 32.0, 31.8, 29.7,27.2, 26.2. **IR spectrum (ATR)**: ν_{max} [cm^{-1}] = 2949, 2867, 1700, 1661, 1593, 1532, 1504, 1397, 1343, 1336, 1233, 1183, 1111, 1015, 872, 829, 783, 762. **UV-Vis spectrum (CD_2Cl_2)**: λ_{max} [nm] (ε [$M^{-1}cm^{-1}$]) = 401 (8,583). **High Resolution Mass (ESI)**: $[M]^+$: calculated: 791.4662, found: 791.4639, discrepancy: -2.9 ppm.

N-Cyclohexyl-3,4-([b]-N,N-bis(p-2,4,4-trimethylpentane-2-yl)phenyl-1-hexyl-1H-indole-6-amine)-1,8-naphthalene dicarboximide

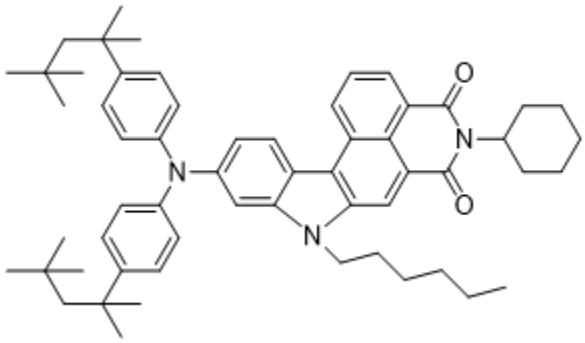

550 mg of N-cyclohexyl-4-(4-bis(*p*-2,4,4-trimethylpentane-2-yl)phenyl-amino-2-nitrophenyl)-naphthalene 1,8-dicarboximide (0.694 mmol) and 545 mg of triphenylphosphine (2.08 mmol) were dissolved in 10 mL of *o*-dichlorobenzene and stirred at 182 °C and 300 W in the microwave (CEM, DISCOVER-S with external pressurised air cooling) for 8 h. After removing the solvent under reduced pressure, the crude product was isolated via column chromatography on silica with dichloromethane and used directly for the next step. **Yield (crude)**: 430 mg orange solid (82%).

350 mg of N-cyclohexyl-3,4-([*b*]-N,N -bis(*p*-2,4,4-trimethylpentane-2-yl)phenyl-1*H*-indole-6-amine)-1,8-naphthalene dicarboximide (0.460 mmol) and 14 mg of sodium hydride (0.583 mmol) were mixed in a Schlenk tube. 15 mL of anhydrous dimethylformamide was added under argon. The solution was stirred for 30 minutes at room temperature. 230 mg of bromohexane (1.39 mmol) was added, and the solution was stirred for another 3 h. After quenching the reaction with water, the solution was washed with water and hydrochloric acid (3:1), extracted with dichloromethane, and dried over magnesium sulfate. The crude product was purified via column chromatography on silica with dichloromethane. **Yield**: 270 mg orange solid (71%).

^{1}H-NMR (700 MHz, THF, 298 K): δ [ppm]: 9.08 (d, J = 8.0, 1H), 8.77 (s, 1H), 8.51 (d, J = 8.8, 1H), 8.46 (d, J = 6.8, 1H), 7.86 (t, J = 7.8, 1H), 7.35 (d, J = 8.6, 4H), 7.23 (d, J = 1.7, 1H), 7.12 (m, 5H), 5.09 (t, J = 12.1, 1H), 4.43 (t, J = 7.1, 2H), 2.73 - 2.61 (m, 2H), 1.89 (d, J = 13.1, 2H), 1.84 - 1.69 (m, 9H, partially overlaid with solvent), 1.51 - 1.24 (m, 21H), 0.88 - 0.78 (m, 21H). **^{13}C-NMR (176 MHz, THF, 298 K)**: δ [ppm]: 165.7, 165.6, 149.2, 146.6, 146.1, 143.9, 139.0, 128.6, 128.5, 128.0, 125.4, 124.63, 121.19,

120.94, 118.8, 116.7, 104., 58.3, 55.3, 54.5, 44.0, 39.4, 33.5, 33.0, 32.7, 32.4, 30.8, 30.4, 28.1, 28.0, 27.0, 23.8, 14.8. **IR spectrum (ATR)**: ν_{max} [cm^{-1}] = 2950, 2927, 2859, 1690, 1648, 1607, 1584, 1505, 1460, 1384, 1316, 1256,1218, 1180, 1101, 1078, 890, 826, 795, 777, 739. **UV-Vis spectrum (CH_2Cl_2)**: λ_{max} [nm] (ε [$M^{-1}cm^{-1}$]) = 489 (26,264). **High Resolution Mass (ESI)**: $[M]^+$: calculated: 843.5703, found: 843.5731, discrepancy: 3.3 ppm. **Elemental analysis ($C_{58}H_{73}N_3O_2$)**: calculated: 82.52% C, 8.72% H, 4.98% N; found: 81.78% C, 8.67% H, 5.07% N.

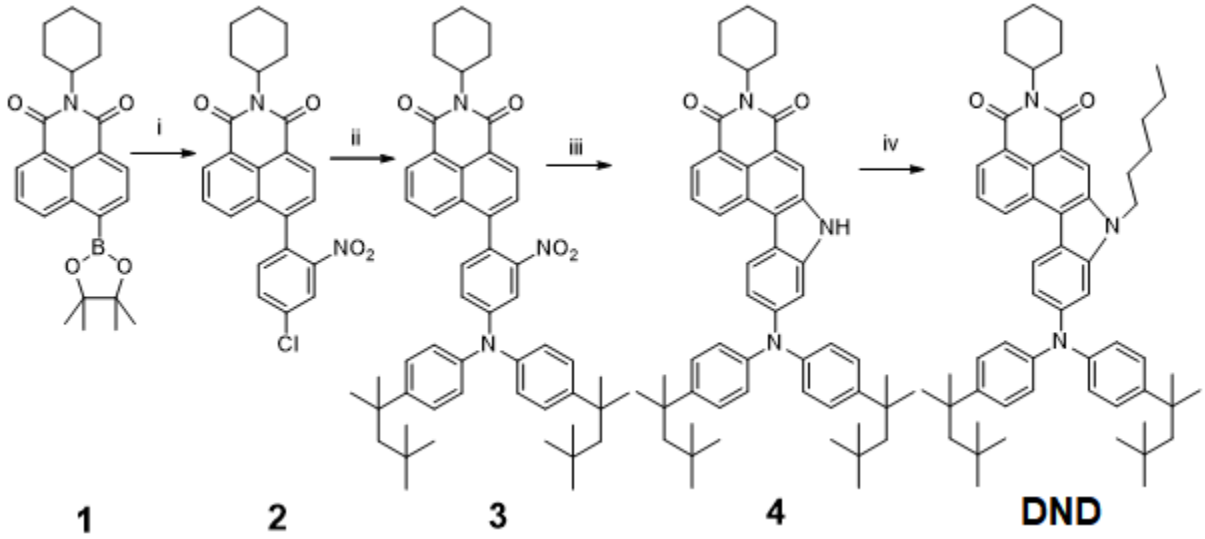

i) K_2CO_3, $Pd(PPh3)_4$, toluene, water, ethanol, 80 °C, 60 h, yield: 32%; ii) (*p*-2,4,4-trimethylpentane-2-yl-phenyl)amine, caesium carbonate, $Pd_2(dba)_3$, BINAP, toluene, 100 °C, 16 h, yield: 64% iii) triphenylphosphine, o-dichlorobenzene, microwave (300 W, 182 °C, 8 h), yield: 82%; iv) NaH, DMF, bromohexane, r.t., 3 h, yield: 71%.

The target DND was obtained via a four-step reaction starting from a carbon-carbon Suzuki coupling. Mixing pinacol boronate functionalized naphthaleneimide **1** with bromo-4-chloro-2-nitrobenzene, palladium catalyst, toluene, water, and ethanol at 80 °C for 2.5 days yielded **2** in 32%. **2** and di(*p*-octylphenyl)amine were then reacted under the Buchwald-Hartwig amination condition to generate 3 in 64% yield. Subsequently, a microwave reactor treated **3** and triphenylphosphine in o-dichlorobenzene leading to **4** in 82%. Owing to its reasonable solubility, **4** could be further alkylated by hexylbromide and

NaH in DMF, which formed the final product DND in 71%. The structures of compounds **1-4** and DND were proved by H-NMR, C-NMR, IR, and Mass spectroscopies.

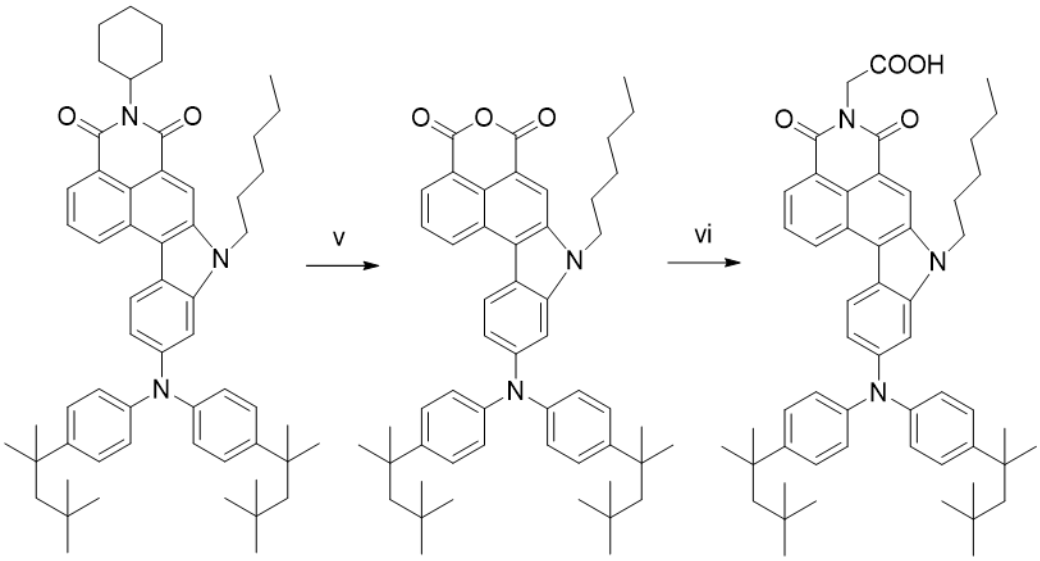

v) 2-methyl-2-butanol, KOH, reflux, overnight, yield: 95%; vi) glycine, imidazole, 140 °C, overnight, yield: 87%.

N-Carboxymethyl-3,4-([*b*]-N,N-bis(*p*-2,4,4-trimethylpentane-2-yl)phenyl-1H-indole-6-amine)-1,8-naphthalene dicarboximide

170 mg of N-cyclohexyl-3,4-([*b*]-N,N -bis(p-2,4,4-trimethylpentane-2-yl)phenyl-1H-indole-6-amine)-1,8-naphthalene dicarboximide (0.201 mmol) was dissolved in 10 mL of 2-methyl-2-butanol. 450 mg of potassium hydroxide (8.04 mmol) was added, the reaction mixture degassed and refluxed under argon overnight. The reaction mixture was poured into an ice water/acetic acid mixture (10:2). The precipitate was filtered, washed with water, and after drying dissolved in dichloromethane. 1-2 mL of acetic acid was added, and the solution was stirred for 1-2 days. After removal of the dichloromethane under reduced pressure, methanol was added. The precipitate was filtered and washed with methanol. The formed anhydride was used directly for the next step without further purification. **Yield (crude)**: 145 mg red solid

(95%).

80 mg of the crude anhydride 5 (0.104 mmol), 1 g of glycine (13.4 mmol), and 2 g of imidazole (29.4 mmol) were mixed in a Schlenk tube and stirred under argon at 140 °C overnight. After cooling down, dilute hydrochloric acid (water:acid (5:1)) was added. The precipitate was filtered and washed with water. The crude product was purified by column chromatography on silica gel with dichloromethane, tetrahydrofuran, and acetic acid. **Yield**: 75 mg orange solid (87%).

^{1}H-NMR (700 MHz, THF, 298 K): δ [ppm]: 9.10 (d, J = 8.3, 1H), 8.72 (s, 1H), 8.50 (d, J = 8.8, 1H), 8.46 (d, J = 7.2, 1H), 7.86 (t, J = 7.8, 1H), 7.36 (d, J = 8.6, 4H), 7.23 (d, J = 1.7, 1H), 7.15 - 7.10 (m, 5H), 4.83 (s, 2H), 4.41 (t, J = 7.2, 2H), 1.83 - 1.77 (m, 6H), 1.40 (s, 12H), 1.32 - 1.24 (m, 6H), 0.88 - 0.77 (m, 21H). **^{13}C-NMR (176 MHz, THF, 298 K)**: δ [ppm]: 167.0, 164.9, 164.8, 149.3, 146.6, 146.2, 144.0, 138.8, 130.5, 128.8, 128.5, 128.3, 128.0, 125.5, 125.4, 124.7, 124.4, 121.7, 119.8, 118.8, 118.7, 116.9, 104.3, 58.3, 44.1, 41.9, 39.4, 33.5, 33.0, 32.7, 32.4, 30.8, 28.1, 23.8, 14.8. **IR spectrum (ATR)**: ν_{max} [cm^{-1}] = 2946, 2867, 1721, 1695, 1661, 1623, 1589, 1513, 1464, 1389, 1358, 1294, 1245, 1178, 1090, 825, 773, 738. **UV-Vis spectrum (CH_2Cl_2)**: λ_{max} [nm] (ε [$M^{-1}cm^{-1}$]) = 335 (26,910), 502 (25,252). **High Resolution Mass (ESI)**: $[M]^+$: calculated: 819.4575, found: 819.4980, discrepancy: 0.6 ppm. **Elemental analysis ($C_{54}H_{65}N_3O_4$)**: calculated: 79.08% C, 7.99% H, 5.12% N; found: 78.64% C, 8.21% H, 5.00% N.

Supplementary Note 2. Steady-state spectroscopic data and the fluorescence lifetime

Measurement of absolute fluorescence quantum yield

The fluorescence quantum yield was calculated using the following equation,[1]

$$\Phi_{fl} = \frac{N_{em}}{N_{abs}} = \frac{E_A - E_B}{S_B - S_A} \qquad \text{(S1)}$$

where Φ_{fl} represents the absolute fluorescence quantum yield of the sample, N_{abs} and N_{em} are the number of photons that absorbed or emitted, respectively, the subscripts A and B represent the sample and the blank (i.e. neat solvent filled in a cell), respectively, S is the area of the excitation pulse within the bandwidth of the pulse, and E corresponds to the integrated area of each emission band.

To estimate the rate constant of non-radiative deactivation (k_{nr}), we used the following equation.

$$k_{nr} = (1 - \Phi_{fl}) / \tau_{fl} \qquad \text{(S2)}$$

where Φ_{fl} is the fluorescence quantum yield calculated by equation (S1) and τ_{fl} is a fluorescence lifetime obtained from TCSPC.

Supplementary Note 3. Details on DFT and TDDFT results

The comparison of various functionals and basis sets with the solvents for the electronic transitions, structural parameters, and dipole moments are shown in Tables S1 – S5. The detailed methods for DFT and TDDFT are described in the Experimental Methods.

Supplementary Note 4. Broadband transient absorption experiments and data analysis

Singular value decomposition (SVD) analysis and kinetic modelling

The broadband transient absorption setup and experimental conditions are described in the Experimental Methods. The singular value decomposition (SVD) analysis was applied for kinetic analysis of transient absorption (TA) spectra. The method for SVD analysis is described in previous publications.[2-4] By the global fitting of the right-singular values (rSVs), which corresponds to time-dependent absorbance change, the TA data sets of THF and DMSO were fit with four time constants, which are summarized in Table 2. Based on the four time constants and four spectrally distinct intermediates, we assumed a sequential

kinetic model.[5]

$$A \xrightarrow{\tau_1} B \xrightarrow{\tau_2} C \xrightarrow{\tau_3} D \xrightarrow{\tau_4} GS \qquad \text{(S3)}$$

We implemented a principal component analysis (PCA) following the sequential kinetic model whereby the experimental TA spectra were decomposed into four species-associated difference spectra (SADS)[6] according to the four species.

$$-\Delta T/T(\mathrm{t},\lambda) = \sum_{i}^{4} C_i^*(t) \cdot SADS_i(\lambda)$$
$$C_i^*(t) = C_i^{SADS}(t) \otimes \mathrm{IRF}(\mathrm{t},\sigma) \qquad \text{(S4)}$$

where $-\Delta T/T(t, \lambda)$ is the theoretical TA spectra at given time delays and wavelengths, $SADS_i(\lambda)$ is the SADS for the i^{th} species, and $C_i^*(t)$ is the time-dependent population of the i^{th} species, which is obtained by the convolution with the instrumental response function (IRF(t,σ)) of the experiment. The discrepancy between the theoretical and experimental TA spectra was minimized via the Nelder-mead simplex method.

Excitation wavelength dependence on ICT dynamics.

We performed TA measurements to investigate the excitation wavelength dependence of DND in DMSO after 400 nm and 473 nm excitation (Figure S7a and S7b), assigned to the $S_0 \rightarrow S_2$ transition and the $S_0 \rightarrow S_1$ transition from the TDDFT calculations, respectively. The overall spectral changes accompanying with the rise of new ESA around 530 − 580 nm are almost identical for both excitation conditions (Figure S7c and S7d), but the kinetics upon 400 nm excitation shows an additional time constant of 61 fs, which is attributable to the internal conversion from S_2 to S_1 due to the excess energy of ~0.48 eV by an excitation pulse (Figure S7e). We can confirm that the dependence on the photon energy of the pump pulse is absent below 3.10 eV of the excitation photon energy and the additional deactivation pathways such as the intersystem crossing from the S_2 state can be excluded.

Supplementary Note 5. Photovoltaic performance of DND

The charge carrier dynamics observed with broadband TA spectroscopy in this work suggest that the intramolecular charge transfer occurring in the excited states of DND would facilitate the charge injection into the electron acceptor when applied to solar cells. While the DND dye would be attached to an external electron acceptor (for example, TiO_2) in the solar cell, the electron will be easily injected to the acceptor at their interface due to the intrinsic electron-donating character of N-annulated rylene, as evidenced by the ultrafast formation of the CS state. Also, the CS state generated in DND can help to enhance the performance of photovoltaics.[7, 8]

To examine the performance of DND in a solar cell, we fabricated the DSSC film using DND as a photosensitizer and characterized its performance. To facilitate the attachment of DND onto the TiO_2 surface, we substituted the cyclohexyl group in dicarboximide moiety with the carboxymethyl group to form DND-1. The details of the fabrication of DSSC are summarized in the Experimental Methods. The absorption spectra and the device efficiencies are presented in Figure S10. Figure S10a and 10b indicate the absorption spectra of DND-1 in THF and DND-1 attached to the TiO_2 electrode, respectively. The substitution of the terminal group does not alter the absorption spectrum (Figure S10a), but the absorption spectrum of DND-1 on the TiO_2 electrode shows the prominent spectral red shift (Figure S10b). To estimate the device performance, we tested the cell efficiencies at an irradiance of 100 mW cm^{-2} under AM 1.5G conditions. As can be seen in Figure S10c, the maximum external quantum efficiency (EQE) is 50 % at 520 nm, where the intensity of the sunlight is maximum. The current density-voltage (I-V) curve in Figure S10d) shows an open-circuit voltage (V_{OC}) of 980 mV, a short-circuit current density (I_{SC}) of 5.2 mA cm^{-2}, and a fill factor (FF) of 0.640, giving a PCE of 3.2 %, as summarized in Table S6. The results of the photovoltaic performance indicate that the electron injection from NANDID to the conduction band of TiO_2 occurs effectively, leading to the current generation.

Table S1. The absorption and emission energies (in nm) in the gas phase and three solvents calculated using (TD)DFT/ 6-311++G(d,p) with the IEFPCM method and various functionals. Values in parentheses are the oscillator strengths. The experimental values for the absorption and emission energies (in nm) are listed for comparison.

Absorption						
	PBE0	CAM-B3LYP	ωB97XD	MN12-SX	MN15	Exp.
Gas	485.2 (0.4679)	391.9 (0.7243)	378.2 (0.7471)	517.2 (0.0075) 514.5 (0.3646)[a]	426.4 (0.6315)	-
Cyclohexane	508.2 (0.5679)	405.9 (0.8647)	390.3 (0.8995)	538.1 (0.4689)	443.5 (0.7571)	482.2
Tetrahydrofuran	522.6 (0.5517)	412.3 (0.8496)	395.2 (0.8853)	554.3 (0.4596)	452.3 (0.7384)	480.1
Dimethylsulfoxide	528.4 (0.5505)	415.0 (0.8486)	397.2 (0.8838)	561.0 (0.4588)	455.9 (0.7360)	487.6
Emission						
	TD-PBE0	TD-CAM-B3LYP	TD-ωB97XD	TD-MN12-SX	TD-MN15	Exp.
Gas	603.1 (0.1280)	441.6 (0.7734)	429.6 (0.8074)	-	473.2 (0.6330)	-
Cyclohexane	589.3 (0.3475)	465.4 (0.9461)	452.4 (0.9901)	646.0 (0.2424)	497.2 (0.8007)	504.1
Tetrahydrofuran	603.8 (0.5780)	496.2 (1.1147)	481.8 (1.1616)	654.8 (0.4144)	528.6 (0.9695)	598.7
Dimethylsulfoxide	616.5 (0.6662)	511.9 (1.1832)	496.8 (1.2284)	664.5 (0.4942)	544.4 (1.0405)	670.6

[a] The S_2 state.

Table S2. The absorption energies (in nm) and the dipole moments of DND in the gas phase and three solvents calculated using (TD)DFT/ 6-311G(d,p) or 6-31G(d,p) with the IEFPCM method and various functionals. Values in parentheses and italic are the oscillator strengths and the dipole moments (in D), respectively.

6-311G(d,p)					
	PBE0	CAM-B3LYP	ωB97XD	MN12-SX	MN15
Gas	457.8 , *6.9* (0.4805)	384.8 , *6.4* (0.7471)	372.9 , *6.3* (0.7642)	494.1 , *6.8* (0.4152)	419.8 , *6.5* (0.6487)
Cyclohexane	497.0 , *7.8* (0.5800)	397.7 , *7.2* (0.8876)	384.3 , *7.0* (0.9165)	516.7 , *7.7* (0.5056)	456.0 , *7.3* (0.7717)
Tetrahydrofuran	509.5 , *8.8* (0.5620)	403.0 , *8.0* (0.8704)	388.4 , *7.8* (0.9008)	531.1 , *8.7* (0.4897)	443.1 , *8.1* (0.7514)
Dimethylsulfoxide	514.4 , *9.2* (0.5597)	405.1 , *8.3* (0.8685)	390.1 , *8.1* (0.8990)	536.8 , *9.1* (0.4872)	446.1 , *8.4* (0.7482)
6-31G(d,p)					
	PBE0	CAM-B3LYP	ωB97XD	MN12-SX	MN15
Gas	474.6 , *6.8* (0.4799)	381.4 , *6.4* (0.7596)	369.7 , *6.2* (0.7806)	492.6 , *6.8* (0.4138)	416.7 , *6.4* (0.6529)
Cyclohexane	496.0 , *7.7* (0.5764)	394.3 , *7.1* (0.8971)	381.1 , *7.0* (0.9300)	515.5 , *7.7* (0.5016)	432.4 , *7.2* (0.7719)
Tetrahydrofuran	508.7 , *8.7* (0.5591)	399.6 , *7.8* (0.8791)	385.3 , *7.7* (0.9135)	530.1 , *8.7* (0.4865)	440.0 , *7.9* (0.7515)
Dimethylsulfoxide	513.7 , *9.0* (0.5571)	401.7 , *8.1* (0.8771)	387.0 , *8.0* (0.9116)	536.0 , *9.0* (0.4844)	443.0 , *8.2* (0.7481)

Table S3. The geometric parameters of dihedral angles for C-C-N-C (in º) and C-N bond lengths (in Å) between DPA and NANDID for the ground state and the lowest singlet excited state (S_1/ICT) calculated using (TD)DFT/ 6-311++G(d,p) with the IEFPCM method and various functionals.

S_0-optimized state					
	PBE0	CAM-B3LYP	ωB97XD	MN12-SX	MN15
Gas	32.4 , 1.404	30.8 , 1.406	31.0 , 1.407	32.1 , 1.403	31.5 , 1.409
Cyclohexane	31.7 , 1.403	30.1 , 1.405	30.3 , 1.406	31.3 , 1.402	30.8 , 1.408
Tetrahydrofuran	30.7 , 1.401	29.0 , 1.404	29.3 , 1.405	30.5 , 1.401	29.9 , 1.407
Dimethylsulfoxide	30.0 , 1.401	28.1 , 1.404	28.5 , 1.405	30.1 , 1.401	29.5 , 1.407
S_1-optimized state					
	PBE0	CAM-B3LYP	ωB97XD	MN12-SX	MN15
Gas	70.1 , 1.448	32.7 , 1.388	30.5 , 1.386	-	39.1 , 1.404
Cyclohexane	54.2 , 1.429	30.0 , 1.382	28.1 , 1.381	56.0 , 1.437	35.0 , 1.396
Tetrahydrofuran	43.4 , 1.410	27.2 , 1.375	25.1 , 1.374	47.0 , 1.420	31.9 , 1.388
Dimethylsulfoxide	40.3 , 1.403	25.9 , 1.372	23.8 , 1.371	43.8 , 1.414	30.6 , 1.384

Table S4. The geometric parameters of dihedral angles for C-C-N-C (in º) and C-N bond lengths (in Å) between DPA and NANDID for the ground state calculated using DFT/ 6-311G(d,p) or 6-31G(d,p) with the IEFPCM method and various functionals.

6-311G(d,p)					
	PBE0	CAM-B3LYP	ωB97XD	MN12-SX	MN15
Gas	32.3 , 1.403	30.9 , 1.406	31.2 , 1.407	32.0 , 1.403	31.5 , 1.409
Cyclohexane	31.7 , 1.402	30.3 , 1.405	30.6 , 1.406	31.2 , 1.402	31.1 , 1.408
Tetrahydrofuran	30.6 , 1.401	29.2 , 1.404	29.4 , 1.405	30.4 , 1.401	30.3 , 1.407
Dimethylsulfoxide	29.9 , 1.401	28.3 , 1.403	28.5 , 1.404	30.1 , 1.401	29.9 , 1.407
6-31G(d,p)					
	PBE0	CAM-B3LYP	ωB97XD	MN12-SX	MN15
Gas	32.6 , 1.405	31.6 , 1.407	31.8 , 1.408	32.3 , 1.405	32.3 , 1.412
Cyclohexane	32.1 , 1.404	31.1 , 1.406	31.3 , 1.407	31.6 , 1.404	31.8 , 1.411
Tetrahydrofuran	31.1 , 1.403	30.3 , 1.406	30.4 , 1.407	30.8 , 1.403	31.2 , 1.410
Dimethylsulfoxide	30.5 , 1.402	29.7 , 1.405	29.9 , 1.406	30.5 , 1.403	30.9 , 1.410

Table S5. Electric dipole moments (in D) of the ground state, FC state, and the lowest singlet excited state (S_1/ICT) of DND calculated by (TD)DFT/ 6-311++G(d,p) with the IEFPCM method and various functionals.

Ground state / FC state					
	PBE0	CAM-B3LYP	ωB97XD	MN12-SX	MN15
Gas	6.9 / 24.7	6.5 / 17.6	6.3 / 15.3	6.8 / -	6.5 / 20.6
Cyclohexane	7.9 / 28.0	7.4 / 20.2	7.1 /17.6	7.8 / 29.1	7.4 / 23.6
Tetrahydrofuran	9.0 / 31.3	8.2 / 22.7	7.9 / 19.9	8.8 / 32.8	8.3 / 26.5
Dimethylsulfoxide	9.4 / 32.7	8.6 / 23.7	8.2 / 20.8	9.3 / 34.3	8.7 / 27.6
S_1/ICT state					
	TD-PBE0	TD-CAM-B3LYP	TD-ωB97XD	TD-MN12-SX	TD-MN15
Gas	30.6	17.3	15.8	-	20.5
Cyclohexane	31.5	20.3	18.7	32.9	23.2
Tetrahydrofuran	33.1	23.5	22.0	35.4	26.3
Dimethylsulfoxide	34.1	25.0	23.4	36.6	27.7

Table S6. Optical and electrochemical properties of DND and photovoltaic performance of the cell measured at an irradiance of 100 mW cm^{-2}, simulated AM 1.5G sunlight.

	λ_{max} (nm) / ε ($M^{-1}cm^{-1}$)	LUMO (eV)	HOMO (eV)	Bandgap (eV)	EQE_{max} (%)	V_{OC} (mV)	I_{SC} (mA cm^{-2})	FF (%)	PCE (%)
DND-1	484 / 25,100	-3.1	-4.8	1.7	50	980	-5.2	64	3.2

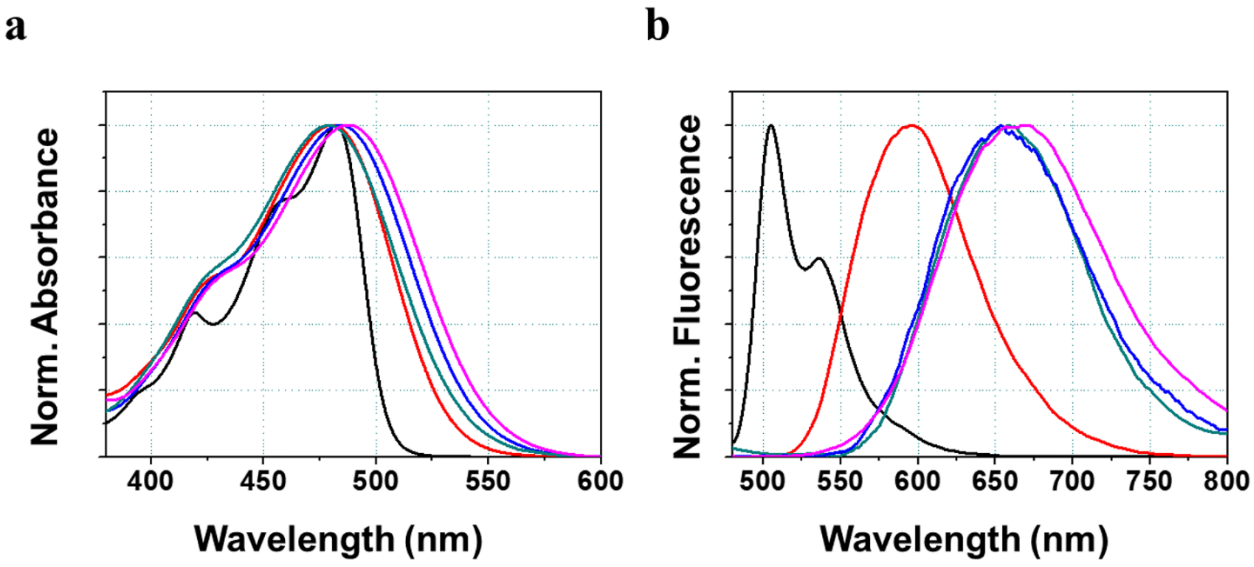

Figure S1. The normalized steady-state (a) absorption and (b) emission spectra with the excitation wavelength of 470 nm of DND in all five solvents: CHX (black), THF (red), DMF (blue), MeCN (dark cyan), and DMSO (magenta).

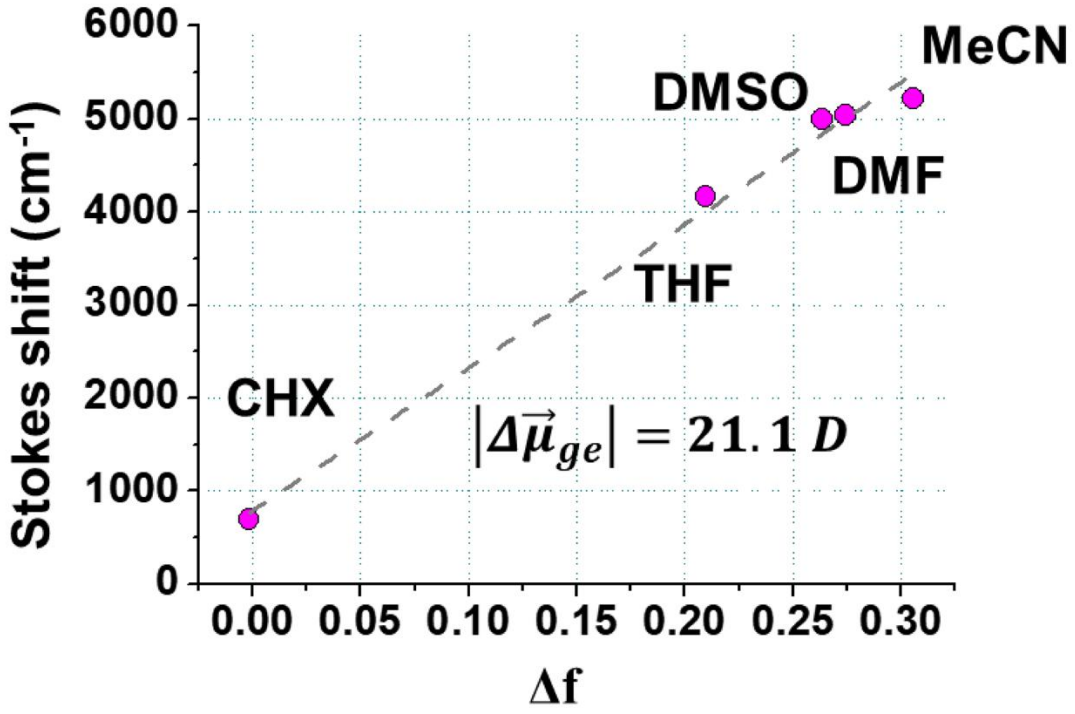

Figure S2. Lippert-Mataga plot for DND in various solvents. The difference of dipole moments between the ground state and the excited state ($\Delta\vec{\mu}_{eg}$) was estimated to be 21.1 D from the slope of the plot. The R^2 of the linear fit is 0.980.

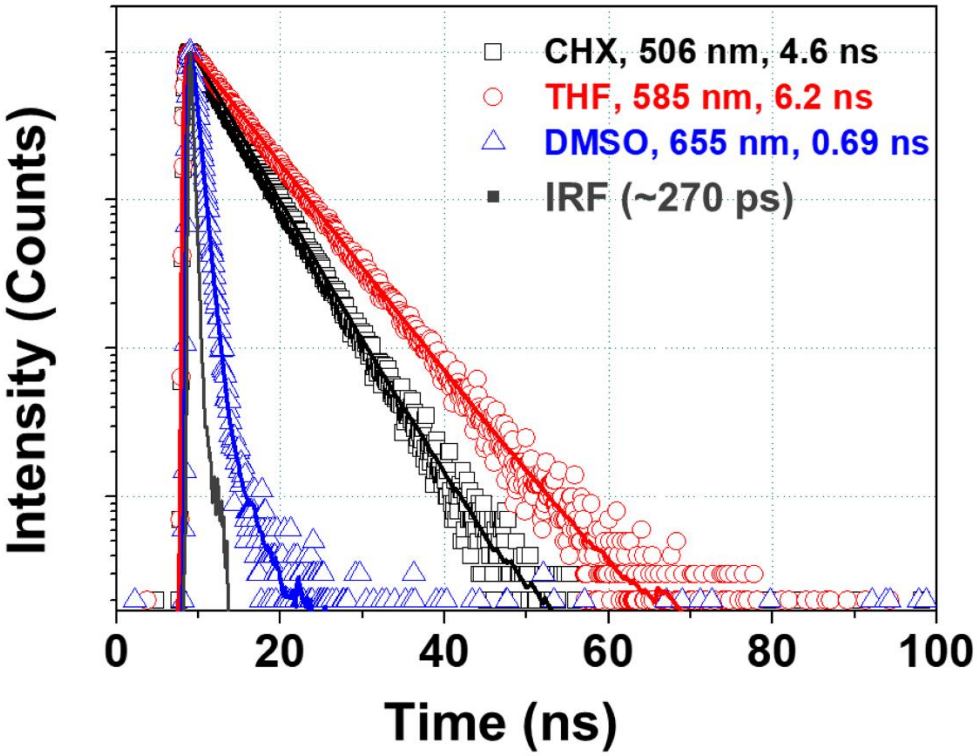

Figure S3. Time-correlated single-photon counting (TCSPC) data of DND in CHX (black, squares), THF (red, circles), and DMSO (blue, triangles) and their fit. The monitored emission wavelength for measurement and fluorescence lifetimes are indicated in the legend. The absorbance was adjusted to below 0.2 at the excitation wavelength of 470 nm for each sample. The instrument response function (IRF) of TCSPC was about 270 ps. The band origin of all monitored emission wavelength is from the lowest emission band and the local emission band is absent in polar solvents.

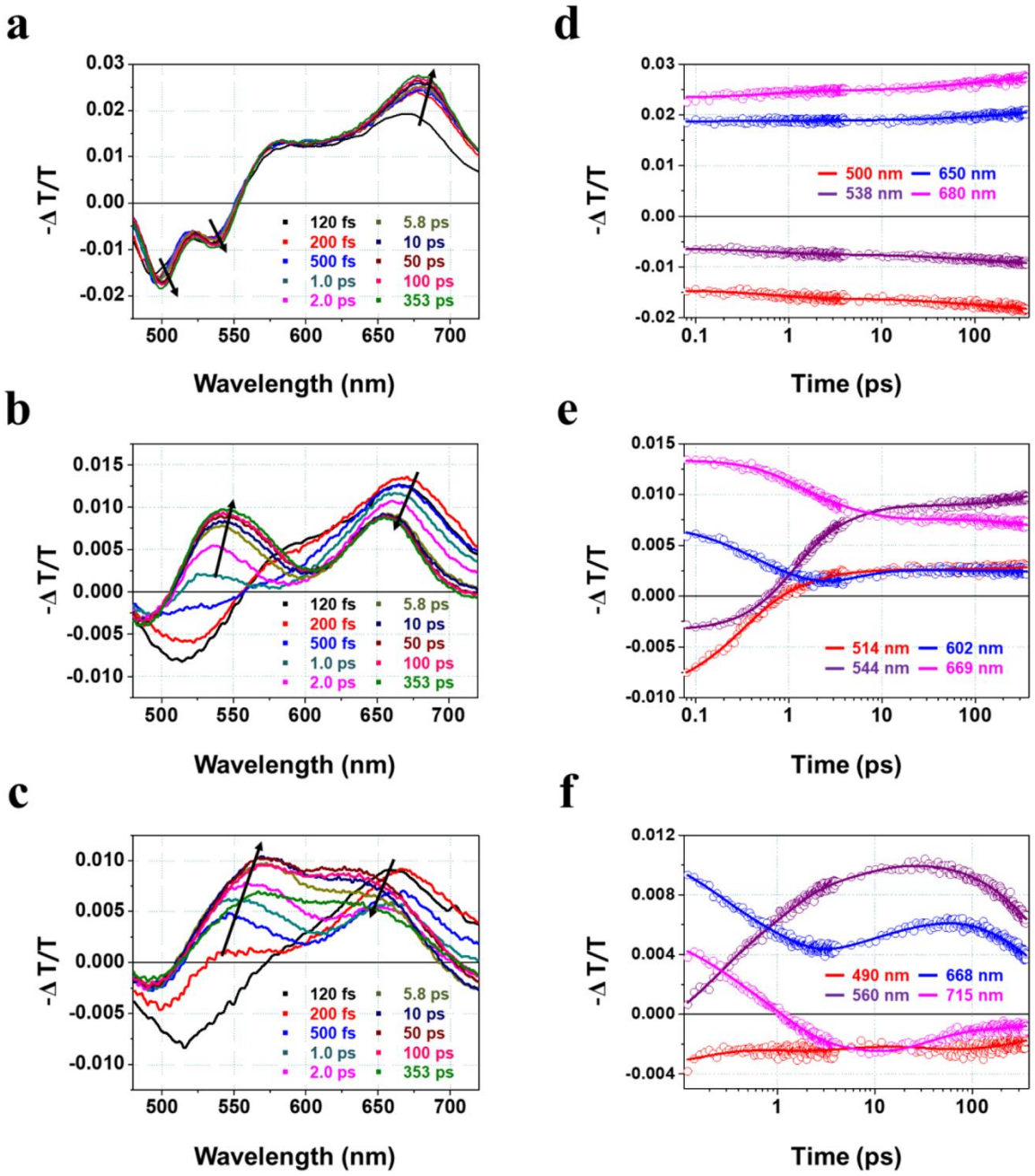

Figure S4. The transient absorption spectra at representative time delays and the kinetics at depicted wavelengths of DND after 473 nm excitation in (a,d) CHX, (b,e) THF, and (c,f) DMSO.

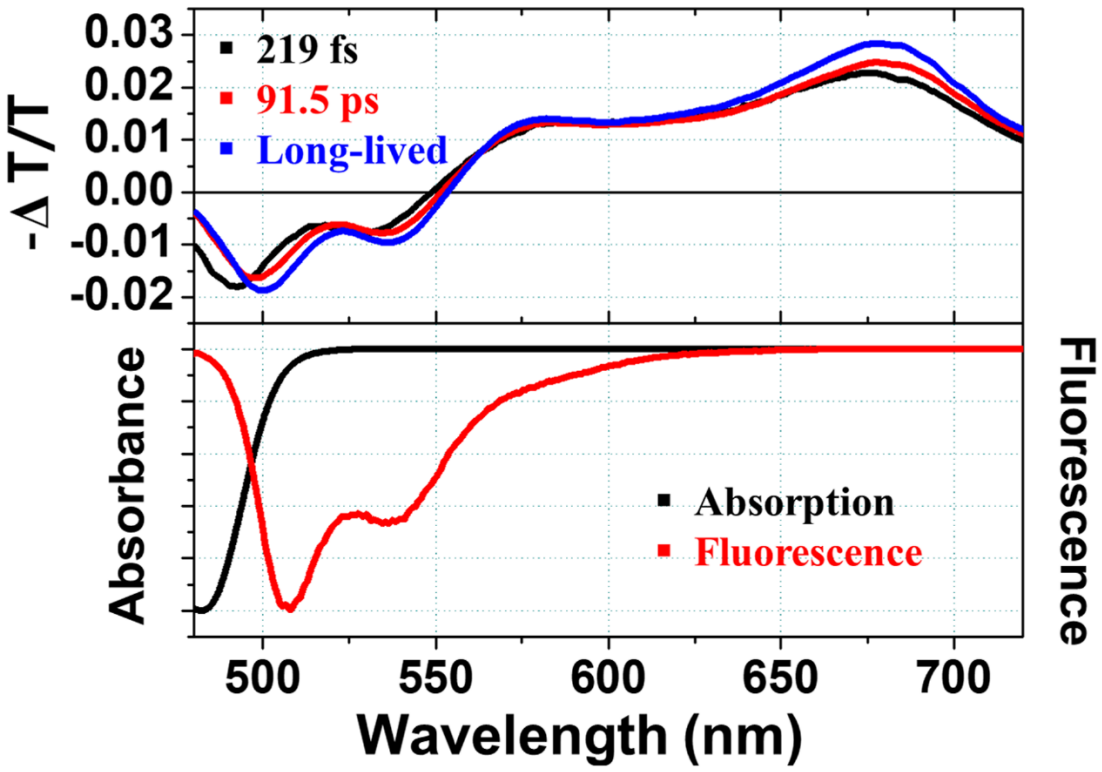

Figure S5. The comparison of peak positions between a steady-state fluorescence spectrum and stimulated emission bands of the 3rd SADS in CHX.

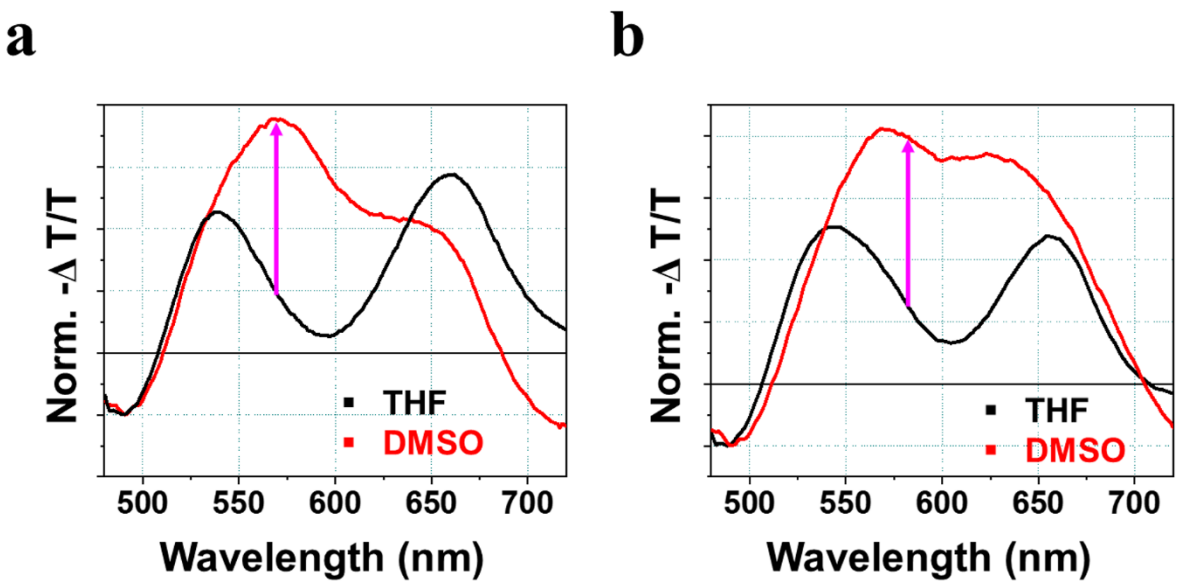

Figure S6. Normalized SADSs divided by GSB for each solvent: THF (black) and DMSO (red) for (a) the 3rd SADS and (b) the 4th SADS. After the 3rd SADS, the growth of ESA is more significant in DMSO, compared with that in THF.

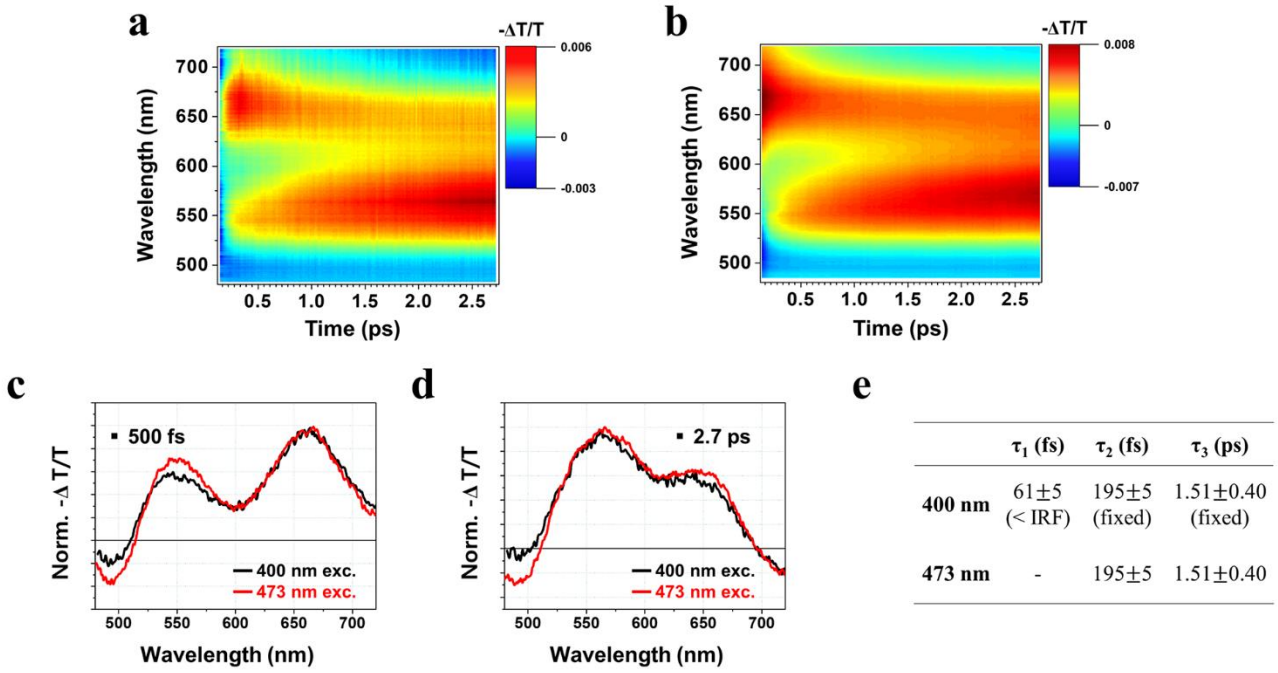

e

	τ_1 (fs)	τ_2 (fs)	τ_3 (ps)
400 nm	61±5 (< IRF)	195±5 (fixed)	1.51±0.40 (fixed)
473 nm	-	195±5	1.51±0.40

Figure S7. Comparison of the ICT dynamics with excitation-wavelength dependence of DND in DMSO measured up to ~3 ps (a) after 400 nm excitation, which is nearly resonant to the $S_0 \rightarrow S_2$ transition and (b) after 473 nm excitation, which is assigned to the $S_0 \rightarrow S_1$ transition based on the TDDFT calculations. The TA spectra upon 400 nm excitation (black) and 473 nm excitation (red) are shown together at the time delays of (d) 500 fs and (e) 2.7 ps for comparison. The kinetic components measured up to ~3 ps are summarized in (e). An additional time constant within IRF is observed upon 400 nm excitation and it is attributable to the internal conversion (IC) from S_2 to S_1. However, the overall excited-state dynamics except for internal conversion and transient spectral features upon 400 nm excitation is similar to that upon 473 nm excitation at the ultrafast time scale regardless of excitation wavelengths.

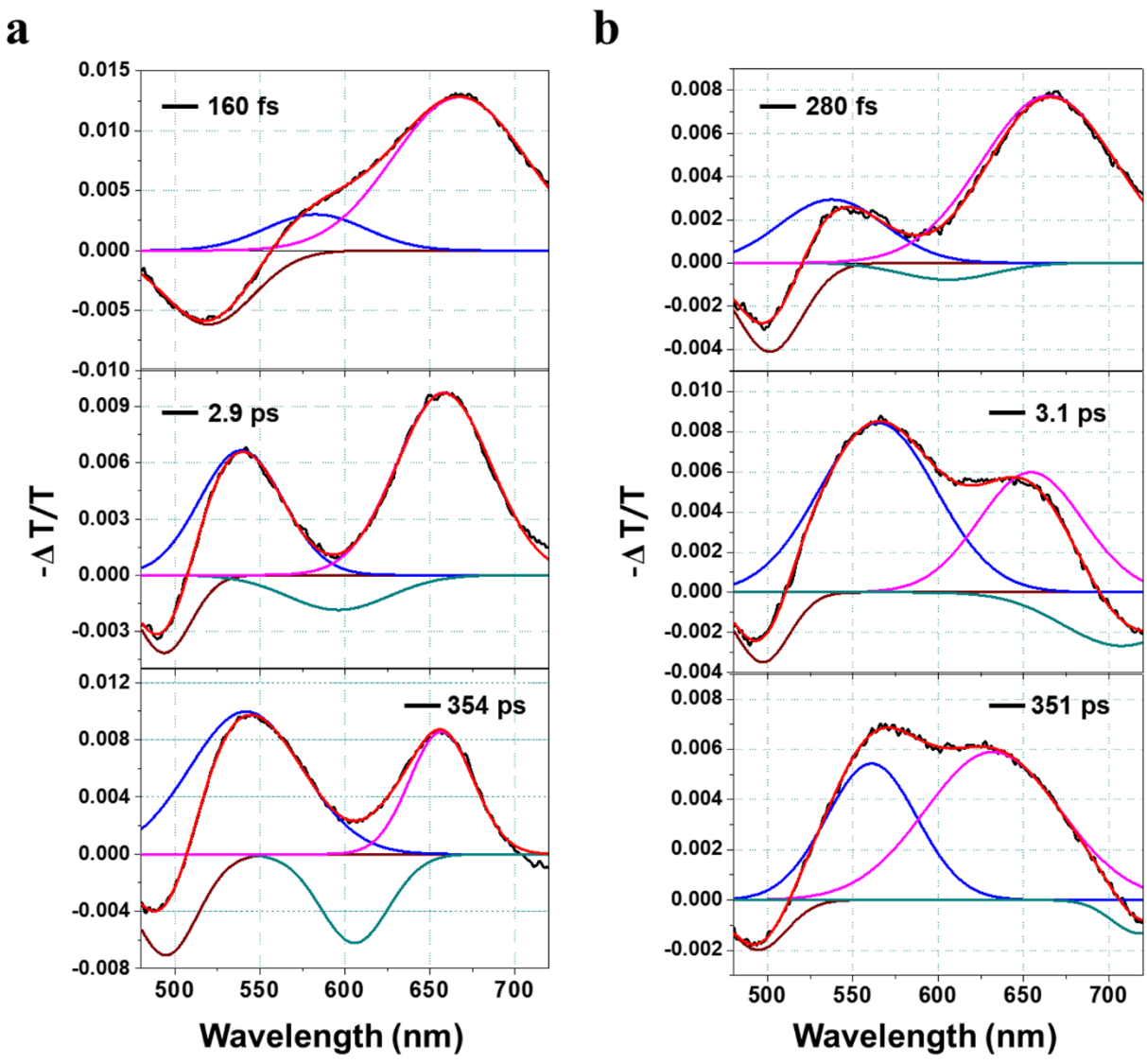

Figure S8. The examples of spectral fitting of transient absorption spectra using the sum of Gaussian functions. The selected TA spectra (black lines) and fits (red lines) of DND in (a) THF and (b) DMSO at specific time delays are shown together with individual Gaussian functions.

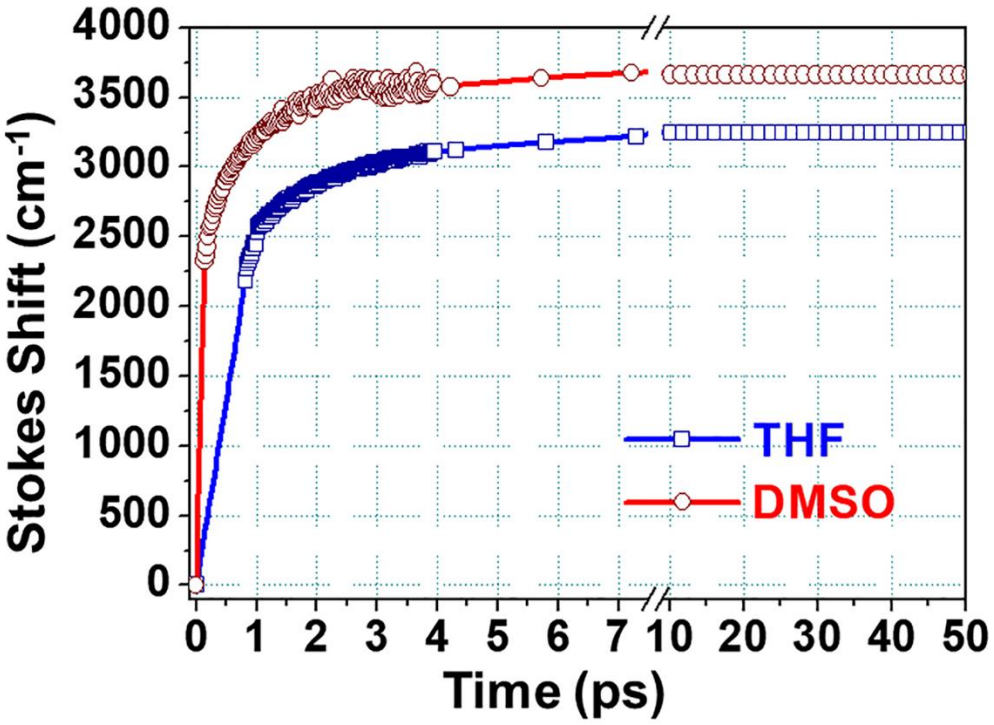

Figure S9. Time evolution of Stokes shift of SE peaks of DND in DMSO (red) and THF (blue).

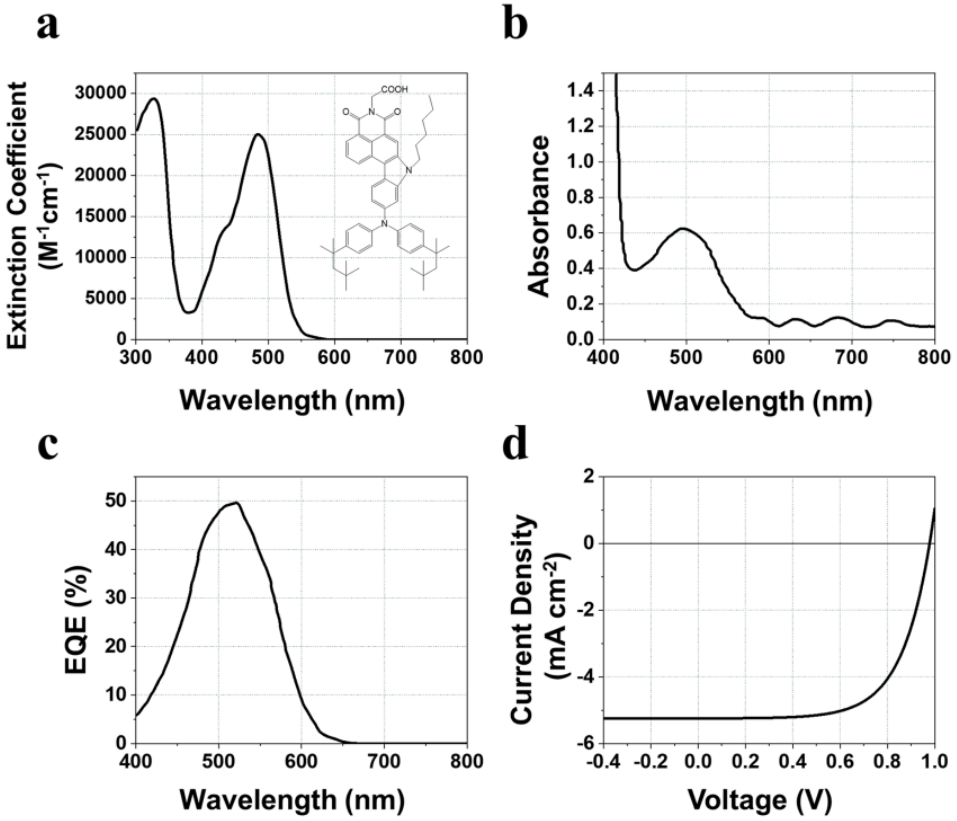

Figure S10. (a) Absorption spectrum of DND-1 in THF. Inset: Molecular structure of DND-1 (b) Absorption spectrum of DND-1 attached to the TiO_2 electrode. (c) Wavelength-resolved EQE spectrum and (d) I-V characteristics of a photovoltaic cell using DND measured under an irradiance of 100 mW cm^{-2}, simulated AM 1.5G sunlight.

Supplementary Note 6. Cartesian coordinates of optimized geometries of DND

The Cartesian coordinates of optimized geometries of DND in the ground state and S_1 state are listed in Table S7 and Table S8, respectively.

Table S7. Ground-state optimized Cartesian coordinates (Å) of DND using MN15/6-311++G(d,p) with the IEFPCM method (in DMSO) level of theory.

Atom	x	y	z
C(1)	-8.351	-4.375	1.207
C(2)	-7.147	5.235	-0.675
C(3)	-2.945	-1.418	-0.692
C(4)	-3.461	-0.197	-0.188
C(5)	-1.588	-1.651	-0.774
C(6)	1.717	-2.672	-1.165
C(7)	1.851	-1.372	-0.624
C(8)	0.752	-0.523	-0.296
C(9)	-0.680	-0.655	-0.367
C(10)	-1.217	0.565	0.117
C(11)	-2.587	0.806	0.224
C(12)	1.006	0.762	0.227
C(13)	3.166	-0.877	-0.392
C(14)	3.370	0.422	0.145

C(15)	2.303	1.240	0.453
C(16)	4.283	-1.684	-0.703
C(17)	4.115	-2.948	-1.232
C(18)	2.821	-3.442	-1.463
C(19)	5.658	-1.187	-0.469
C(20)	4.732	0.930	0.390
N(21)	5.804	0.074	0.107
N(22)	-4.854	-0.009	-0.122
O(23)	6.641	-1.853	-0.764
O(24)	4.930	2.056	0.828
C(25)	7.169	0.575	0.383
C(26)	7.930	0.909	-0.911
C(27)	7.999	-0.321	1.301
C(28)	9.178	0.513	1.830
C(29)	9.442	0.928	-0.643
C(30)	9.713	1.482	0.755
C(31)	-0.375	2.738	1.017
C(32)	-7.441	-3.222	0.875
C(33)	-7.788	-2.289	-0.108
C(34)	-6.214	-3.059	1.523

C(35)	-5.361	-2.006	1.207
C(36)	-6.936	-1.244	-0.446
C(37)	-5.711	-1.092	0.210
C(38)	-6.532	3.870	-0.514
C(39)	-5.555	3.411	-1.405
C(40)	-6.931	3.012	0.513
C(41)	-6.378	1.742	0.653
C(42)	-5.008	2.139	-1.286
C(43)	-5.413	1.292	-0.249
N(44)	-0.190	1.412	0.461
H(45)	-8.192	-4.720	2.230
H(46)	-9.400	-4.096	1.096
H(47)	-8.166	-5.224	0.542
H(48)	-7.559	5.595	0.269
H(49)	-6.413	5.960	-1.030
H(50)	-7.963	5.213	-1.404
H(51)	-3.643	-2.179	-1.021
H(52)	-1.251	-2.601	-1.168
H(53)	0.729	-3.072	-1.353
H(54)	-2.966	1.740	0.622

H(55)	2.496	2.224	0.863
H(56)	4.990	-3.543	-1.462
H(57)	2.690	-4.434	-1.877
H(58)	7.599	1.890	-1.268
H(59)	7.384	-0.691	2.127
H(60)	8.866	1.080	2.713
H(61)	9.845	-0.089	-0.709
H(62)	10.780	1.664	0.907
H(63)	-0.750	2.686	2.041
H(64)	-1.082	3.301	0.405
H(65)	0.573	3.271	1.017
H(66)	-8.738	-2.389	-0.624
H(67)	-5.927	-3.759	2.302
H(68)	-4.419	-1.887	1.732
H(69)	-7.218	-0.532	-1.215
H(70)	-5.226	4.057	-2.213
H(71)	-7.680	3.347	1.225
H(72)	-6.694	1.092	1.462
H(73)	-4.258	1.795	-1.990
H(74)	6.998	1.504	0.929

H(75)	7.691	0.176	-1.684
H(76)	9.951	1.519	-1.409
H(77)	9.217	2.456	0.845
H(78)	8.362	-1.188	0.750
H(79)	9.975	-0.162	2.153

Table S8. S_1-optimized Cartesian coordinates (Å) of DND using TD-MN15/6-311++G(d,p) with the IEFPCM method (in DMSO) level of theory.

Atom	**x**	**y**	**z**
C(1)	-8.285	-4.425	1.096
C(2)	-7.175	5.180	-0.699
C(3)	-2.935	-1.419	-0.619
C(4)	-3.453	-0.185	-0.145
C(5)	-1.580	-1.632	-0.726
C(6)	1.682	-2.650	-1.127
C(7)	1.831	-1.358	-0.613
C(8)	0.733	-0.478	-0.295

C(9)	-0.669	-0.607	-0.352
C(10)	-1.222	0.638	0.111
C(11)	-2.573	0.865	0.224
C(12)	1.007	0.840	0.208
C(13)	3.155	-0.858	-0.383
C(14)	3.363	0.452	0.130
C(15)	2.287	1.316	0.427
C(16)	4.265	-1.683	-0.675
C(17)	4.076	-2.977	-1.191
C(18)	2.798	-3.452	-1.413
C(19)	5.625	-1.208	-0.451
C(20)	4.712	0.940	0.365
N(21)	5.775	0.070	0.089
N(22)	-4.821	-0.002	-0.034
O(23)	6.620	-1.893	-0.718
O(24)	4.927	2.082	0.797

C(25)	7.140	0.566	0.357
C(26)	7.920	0.838	-0.942
C(27)	7.951	-0.299	1.321
C(28)	9.142	0.537	1.822
C(29)	9.429	0.834	-0.666
C(30)	9.704	1.445	0.708
C(31)	-0.341	2.832	0.956
C(32)	-7.386	-3.255	0.811
C(33)	-7.728	-2.301	-0.154
C(34)	-6.173	-3.099	1.494
C(35)	-5.325	-2.037	1.221
C(36)	-6.889	-1.233	-0.442
C(37)	-5.678	-1.099	0.244
C(38)	-6.541	3.829	-0.516
C(39)	-5.521	3.389	-1.366
C(40)	-6.976	2.966	0.499

C(41)	-6.418	1.708	0.663
C(42)	-4.953	2.130	-1.218
C(43)	-5.397	1.284	-0.197
N(44)	-0.188	1.493	0.426
H(45)	-8.244	-4.706	2.150
H(46)	-9.320	-4.202	0.833
H(47)	-7.976	-5.298	0.513
H(48)	-7.411	5.637	0.263
H(49)	-6.518	5.853	-1.253
H(50)	-8.111	5.094	-1.258
H(51)	-3.630	-2.190	-0.927
H(52)	-1.235	-2.580	-1.113
H(53)	0.694	-3.048	-1.314
H(54)	-2.967	1.790	0.624
H(55)	2.490	2.301	0.824
H(56)	4.949	-3.581	-1.406

H(57)	2.648	-4.449	-1.811
H(58)	7.614	1.815	-1.335
H(59)	7.324	-0.619	2.158
H(60)	8.834	1.150	2.674
H(61)	9.808	-0.195	-0.683
H(62)	10.773	1.612	0.860
H(63)	-0.464	2.823	2.042
H(64)	-1.211	3.308	0.501
H(65)	0.537	3.425	0.701
H(66)	-8.664	-2.402	-0.693
H(67)	-5.900	-3.815	2.262
H(68)	-4.398	-1.912	1.769
H(69)	-7.160	-0.504	-1.198
H(70)	-5.175	4.038	-2.163
H(71)	-7.757	3.294	1.176
H(72)	-6.752	1.053	1.460

H(73)	-4.177	1.79	-1.895
H(74)	6.976	1.520	0.860
H(75)	7.667	0.085	-1.691
H(76)	9.958	1.377	-1.453
H(77)	9.226	2.431	0.750
H(78)	8.300	-1.198	0.813
H(79)	9.924	-0.137	2.183

SI References

1. Würth, C.; Grabolle, M.; Pauli, J.; Spieles, M.; Resch-Genger, U., Comparison of methods and achievable uncertainties for the relative and absolute measurement of photoluminescence quantum yields. *Anal. Chem.* **2011,** *83* (9), 3431-3439.

2. Henry, E. R.; Hofrichter, J., Singular Value Decomposition - Application to Analysis of Experimental-Data. *Method Enzymol* **1992,** *210*, 129-192.

3. Ihee, H.; Rajagopal, S.; Srajer, V.; Pahl, R.; Anderson, S.; Schmidt, M.; Schotte, F.; Anfinrud, P. A.; Wulff, M.; Moffat, K., Visualizing reaction pathways in photoactive yellow protein from nanoseconds to seconds. *Proc. Natl. Acad. Sci. U. S. A.* **2005,** *102* (20), 7145-7150.

4. Oang, K. Y.; Kim, J. G.; Yang, C.; Kim, T. W.; Kim, Y.; Kim, K. H.; Kim, J.; Ihee, H., Conformational Substates of Myoglobin Intermediate Resolved by Picosecond X-ray Solution Scattering. *J. Phys. Chem. Lett.* **2014,** *5* (5), 804-808.

5. Kim, T. W.; Yang, C.; Kim, Y.; Kim, J. G.; Kim, J.; Jung, Y. O.; Jun, S.; Lee, S. J.; Park, S.; Kosheleva, I.; Henning, R.; van Thore, J. J.; Ihee, H., Combined probes of X-ray scattering and optical spectroscopy reveal how global conformational change is temporally and spatially linked to local structural perturbation in photoactive yellow protein. *Phys. Chem. Chem. Phys.* **2016,** *18* (13), 8911-8919.

6. van Stokkum, I. H.; Larsen, D. S.; van Grondelle, R., Global and target analysis of time-resolved spectra. *Biochimica et biophysica acta* **2004,** *1657* (2-3), 82-104.

7. Rolczynski, B. S.; Szarko, J. M.; Son, H. J.; Liang, Y. Y.; Yu, L. P.; Chen, L. X., Ultrafast Intramolecular Exciton Splitting Dynamics in Isolated Low-Band-Gap Polymers and Their Implication in Photovoltaic Materials Design. *J. Am. Chem. Soc.* **2012,** *134* (9), 4142-4152.

8. Roy, P.; Jha, A.; Yasarapudi, V. B.; Ram, T.; Puttaraju, B.; Patil, S.; Dasgupta, J., Ultrafast bridge planarization in donor-pi-acceptor copolymers drives intramolecular charge transfer. *Nat. Commun.* **2017,** *8*.